ACS OMEGA

http://pubs.acs.org/journal/acsodf

Article

Recyclability of Vitrimer Materials: Impact of Catalyst and Processing Conditions

Amber M. Hubbard,* Yixin Ren, Alireza Sarvestani, Dominik Konkolewicz, Catalin R. Picu, Ajit K. Roy, Vikas Varshney, and Dhriti Nepal*

Cite This: *ACS Omega* 2022, 7, 29125−29134

Read Online

ACCESS | Metrics & More | Article Recommendations | Supporting Information

ABSTRACT: With sustainability at the forefront of material research, recyclable polymers, such as vitrimers, have garnered increasing attention since their introduction in 2011. In addition to a traditional glass-transition temperature (T_g), vitrimers have a second topology freezing temperature (T_v) above which dynamic covalent bonds allow for rapid stress relaxation, self-healing, and shape reprogramming. Herein, we demonstrate the self-healing, shape memory, and shape reconfigurability properties as a function of experimental conditions, aiming toward recyclability and increased useful lifetime of the material. Of interest, we report the influence of processing conditions, which makes the material vulnerable to degradation. We report a decreased crosslink density with increased thermal cycling and compressive stress. Furthermore, we demonstrate that shape reconfigurability and self-healing are enhanced with increasing compressive stress and catalyst concentration, while their performance as a shape memory material remains unchanged. Though increasing the catalyst concentration, temperature, and compressive stress clearly enhances the recovery performance of vitrimers, we must emphasize its trade-off when considering the material degradation reported here. While vitrimers hold great promise as structural materials, it is vital to understand how experimental parameters impact their properties, stability, and reprocessability before vitrimers reach their true potential.

INTRODUCTION

Vitrimers and other dynamic polymer materials hold great promise in various applications ranging from structural materials to coatings and actuators.[1−5] Coupling the strength and stiffness of a thermoset with the processability of a thermoplastic makes vitrimers particularly exciting for the increased push toward polymer sustainability.[3,6−9] For example, recyclable and self-healing polymers can increase the lifetime of materials, allowing one to move away from single-use components.

However, before vitrimers and other covalently adaptable networks (CANs) can be utilized in real-world applications, it is vital to understand how their composition and processing conditions impact their cycle lifetime. Previous research has clearly demonstrated that environmental conditions (e.g., temperature and stress[10−12]) and compositional conditions (e.g., catalyst type and catalyst concentration[11,13,14]) impact vitrimer and vitrimer composite performance.[1,15−17] Primarily, vitrimer characteristic performance can be quantified by measuring the topology freezing temperature (T_v), where these dynamic covalent bond exchange reactions freely occur.[10,11,18−21] To name a few, Capelot et al.[14] initially reported that varying the catalyst composition and increasing its concentration can decrease the T_v. In addition, Kaiser et al.[10] and our previous research[11] confirm that increasing stress on the sample and decreasing the sample heating rate both quantitatively decrease the T_v. Overwhelmingly, it is clear that catalyst composition and concentration are the two primary factors determining vitrimer performance.

While these fundamental impacts are well documented, the effect on overall applicability is far less understood. Herein, we discuss how compositional and environmental factors impact the self-healing, shape memory, shape reconfigurability, and overall network resistance of vitrimer materials. For example, to the authors' knowledge, quantified changes in shape reconfigurability as a function of catalyst concentration and stress on the same are yet to be explored. We should, at this time, note the difference between self-healing, reprogramming, and reprocessing. While the mechanism behind these methods is the same (dynamic covalent bond exchange reaction), they are phenomenologically different. Self-healing corrects damage

Received: May 15, 2022
Accepted: July 25, 2022
Published: August 9, 2022

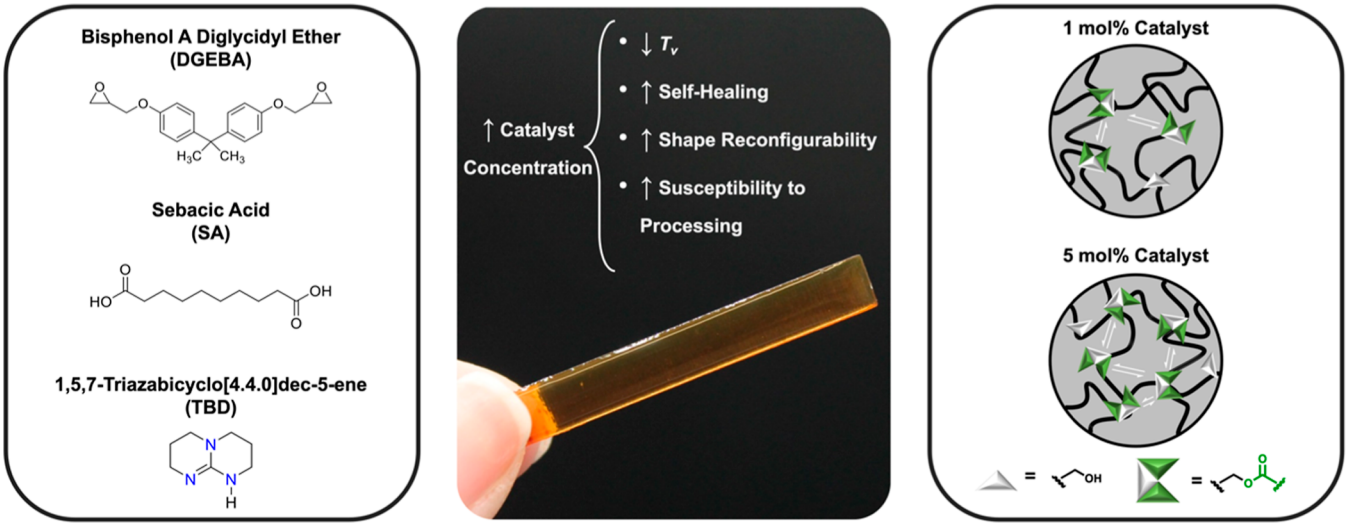

Figure 1. As the catalyst concentration increases, the number of transesterification reactions increases per unit time and per unit volume. This increase in catalyst concentration results in a direct increase in self-healing and shape reconfigurability while also making the material susceptible to property degradation as a function of processing conditions. All chemical structures are depicted in the far-left panel, where bisphenol A diglycidyl ether is an epoxy resin, sebacic acid is a crosslinker, and 1,5,7-triazabicyclo[4.4.0]dec-5-ene is the catalyst molecule. The dynamic covalent reaction site (ester activated via TBD) is seen as the geometric structures (white and green) in the far-right panel.

inflicted upon the sample in the form of scratches, cuts, or internal damage accumulated in service.[12,22−24] Reprogramming/reconfigurability transforms the material to a new permanent shape with the material not being broken down (e.g., palletization, melting, etc.), which will be discussed in a later section.[16,18,25,26] Finally, reprocessing breaks down the polymer materials for regeneration of a new sample, which is outside the scope of this work.[1,2,23,27−31] It is worth noting that shape memory is similar to reprogramming, where instead of a new permanent shape, the polymer material is programmed into a temporary shape.

While shape memory capability does not appear to be significantly impacted by catalyst concentration or applied stress on the sample, the same cannot be said for either self-healing or shape reconfigurability. This correlation is reasonable given the fact that shape memory behavior takes advantage of the matrix's glass transition temperature (T_g) or melt temperature (T_m), while self-healing and shape reconfigurability take advantage of the T_v. We demonstrate, for the first time, that increasing the catalyst concentration can make the vitrimer network susceptible to a decreased crosslink density and T_g as a result of cyclic processing with compressive stress; this finding is in direct opposition to the commonly held notion that vitrimers maintain a constant crosslink density with processing. Although vitrimers demonstrate cyclic healing behavior, understanding and quantifying their susceptibility to network structure and physical property changes throughout these cycles are essential to using vitrimers in their diverse range of potential applications.

RESULTS AND DISCUSSION

Herein, we demonstrate the effect of processing (i.e., repeated thermal cycling and the application of compressive stress) on material performance in the presence of a catalyst of various concentrations. It should be noted that we only explore one vitrimer chemistry to fully understand the impact of each experimental parameter and additional vitrimer chemistries will be explored in future work. Throughout this work, the dynamic covalent bond exchange reaction is a transesterification reaction, as detailed in the Materials and Methods section where the components of this vitrimer material are seen in Figure 1.[4,6,8,9,11,32] Overall, we report that increasing the catalyst concentration decreases the T_v and increases the vitrimer's processability (cf. Figure 1).

Mechanical Characterization and Self-Healing. First, it is important to characterize the properties (i.e., mechanical and thermomechanical) of the neat vitrimer material. As previously reported, the T_g changes minimally with variations in catalyst concentration with a value of around 35 °C for a sample with a 5 mol % concentration.[11] Meanwhile, the T_v decreases with increasing catalyst concentration with a value of around 250 and 200 °C for samples with a 1 and 5 mol % catalyst concentration, respectively (cf. Figure S1). In the absence of a catalyst, the T_g is noticeably higher, around 53 °C, and there is no reported T_v. This trend of decreasing T_g with increasing catalyst concentration makes sense as the crosslink density is shown to be indirectly related to the catalyst concentration (cf. Figure S2). These transition temperatures (T_g and T_v) are the key parameters dictating the shape memory and shape reconfigurability behavior of the material, respectively. Shape memory can be achieved by cycling above and below the T_g only, while shape reconfigurability involves cycling above and below the T_v.

In addition, we also demonstrate a decrease in mechanical properties with increasing catalyst concentration (Young's modulus of 1.7 and 1.1 GPa for samples with 0 mol % or 5 mol % catalyst concentration, respectively), where all tested materials exhibit ductile behavior and necking, as seen in Figure S1.[33] Modulus values agree well with previous literature (e.g., Young's modulus values of 0.56−1.6 GPa)[2,16,29] and the inverse relationship between catalyst concentration and mechanical properties is consistent with dynamic mechanical analysis (DMA) data presented in our previous work,[11] along with the resulting values for molecular weight between crosslinks (cf. Figure S2).

A key application space for vitrimer materials is self-healing, which takes advantage of the dynamic covalent bond exchange

https://doi.org/10.1021/acsomega.2c02677
ACS Omega 2022, 7, 29125−29134

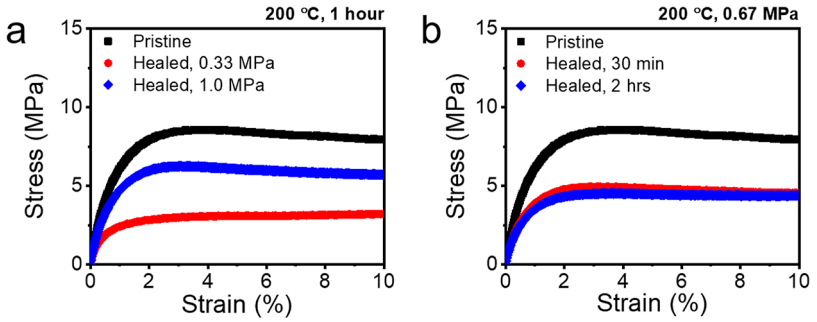

Figure 2. Representative mechanical testing data are shown comparing pristine vitrimer materials with those that have been damaged and self-healed. All samples contained a 5 mol % catalyst concentration, and a minimum of five samples were tested to achieve normal statistical distribution. (a) Samples are healed in a hot press at 200 °C for 1 h, with varying pressures; unsurprisingly, increasing the pressure increases the degree of healing and recovery of mechanical properties. (b) Samples are healed in a hot press at 200 °C under 0.67 MPa of pressure, with varying times. The length of time appears to have a negligible impact on the degree of self-healing; this trend is reasonable as both times exceed the stress relaxation constant for these materials, as previously reported.[11]

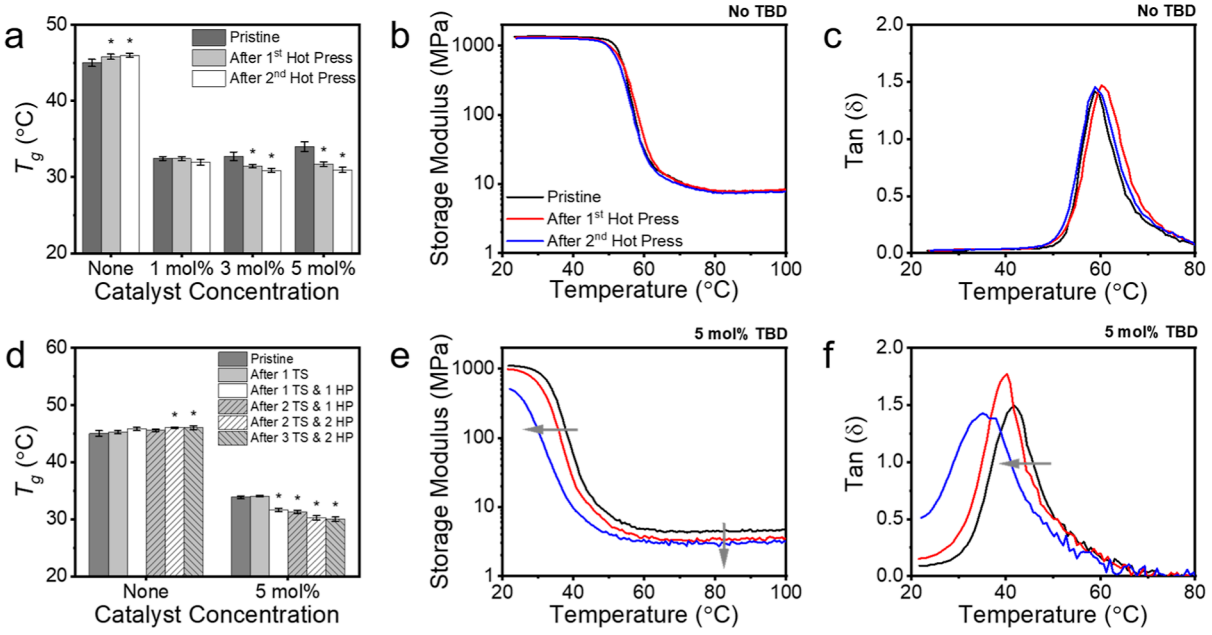

Figure 3. (a) Changes in the T_g are determined via DSC for a variety of catalyst concentrations after a series of HP. (d) Similar results are reported for samples after a series of temperature sweep experiments cycled with HP. The sample size is four to ensure statistical significance; bars denoted with * indicate statistical significance ($p < 0.05$). The temperature sweep results are reported for samples with no catalyst (b–c) and for samples with a 5 mol % catalyst concentration (e–f) as the storage modulus (b,e) and tan(δ) curves (c,f).

reaction at elevated temperatures. In Figure S3, we show that self-healing (cf. Figure S4) fails in the absence of a catalyst and succeeds in its presence. To quantify this healing behavior, we perform tensile tests on both pristine samples and samples that have been cut and healed (cf. Figure 2). It is reasonable to assume that the relevant experimental parameters in determining the degree of self-healing are time, temperature, pressure, and surface area contact between the healing surfaces.[12,23,29,34] For clarity, we only vary pressure and time in this study and attempt to measure the change in mechanical response as a function of healing for a sample with a 5 mol % catalyst concentration. Comparing the tensile test results of pristine and healed samples shows reasonable recovery.

As expected, increasing the applied pressure during hot pressing (HP) increases the degree of self-healing and recovery of mechanical properties (cf. Figure 2a). Previous research has demonstrated that the transesterification reaction is stress-favored,[10,11] so that increases in stress should increase the rate of transesterification reactions; additionally, it is reasonable to assume that increasing the compressive stress will increase the surface area contact between the two healing surfaces.

Interestingly, increasing the hot press time does not appear to significantly impact the degree of self-healing and recovery of mechanical properties for these pressure and temperature conditions (cf. Figure 2b). This makes sense as both times reported (30 min and 2 h) are longer than the stress relaxation constant of samples with a 5 mol % catalyst concentration at 200 °C, reported as ∼95 s in our previous work.[11] It is important to note that we do not see a complete recovery of the mechanical properties (i.e., comparable modulus and yield stress between pristine and healed samples), which is expected given the minor surface scaring as seen in Figure S3b. We postulate that increasing the temperature or pressure would result in full recovery; however, increasing these conditions makes the material vulnerable to network changes, as will be discussed in the next section. We should note that the healing

https://doi.org/10.1021/acsomega.2c02677
ACS Omega 2022, 7, 29125−29134

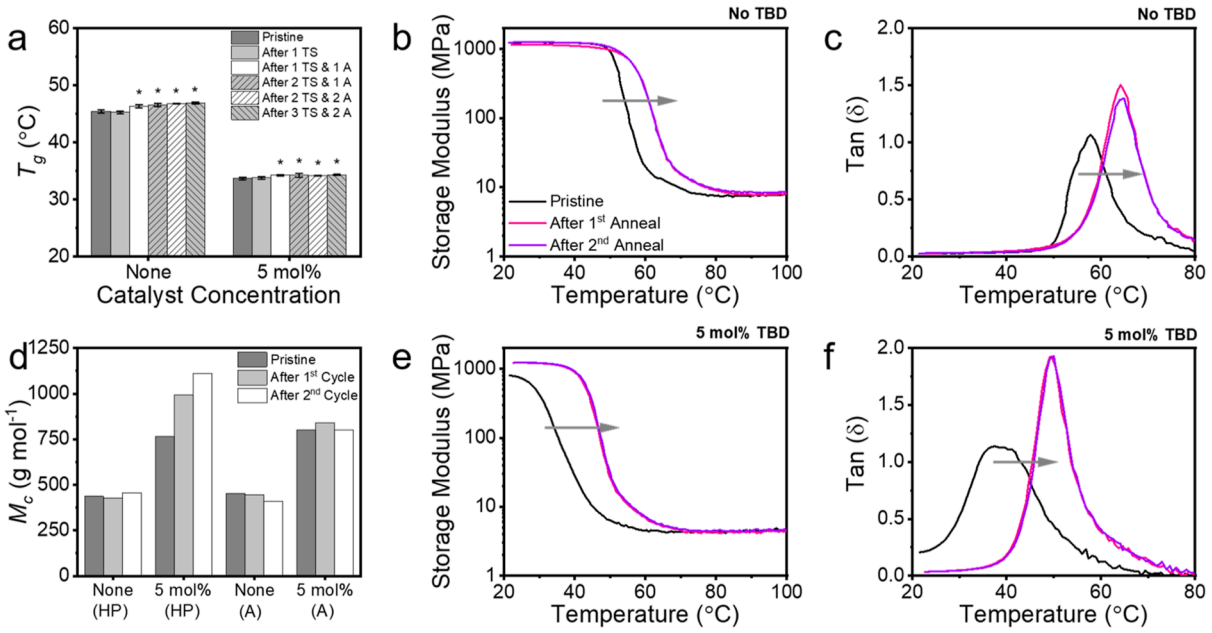

Figure 4. (a) Changes in the T_g are determined via DSC for samples after a series of temperature sweep experiments cycled with annealing. The sample size is four to ensure statistical significance; bars denoted with * indicate statistical significance ($p < 0.05$). (d) The molecular weight between crosslinks is reported for each cycle when the temperature sweeps are cycled between HP or A for samples with and without a catalyst. The temperature sweep results are reported for samples with no catalyst (b−c) and for samples with a 5 mol % catalyst concentration (e−f) as the storage modulus (b,e) and tan(δ) curves (c,f).

times utilized here are significantly shorter than those in previously reported work.[22,24,35]

Impact of Processing Conditions. As demonstrated, a finite amount of pressure must be applied to the sample to achieve self-healing. For example, if vitrimers were simply placed next to each other with time and temperature, no self-healing would be observed in our system (cf. Figure S5). Some softer CANs have previously reported[22,35] not requiring pressure for self-healing due to their tacky/sticky nature, which ensures proper contact between the two respective surfaces. However, for stiffer materials like ours, they will not naturally stick together and therefore require pressure to ensure proper contact. In addition, the applied pressure facilitates self-healing by increasing the effective contact area between the broken surfaces, therefore increasing the opportunities for the polymer chains to cross-diffuse.

It is worth noting that vitrimers are claimed to have constant crosslink density as a function of temperature and processing conditions, which should enable the materials to tolerate the self-healing conditions as has been noted previously in the literature.[9,18,36] However, we report here for the first time that by processing these materials with compressive stress, we see a noticeable change in material properties (e.g., T_g and storage modulus), which is not present in the absence of pressure.

Figure 3a shows how the T_g changes for samples with varying catalyst concentrations when they are repeatedly hot pressed at 200 °C for 1 h under 0.5 MPa. Differential scanning calorimetry (DSC) was performed between each cycle where a minimum of four samples were tested (achieving normal statistical distribution) to determine the ΔT_g with processing. All relevant DSC data are shown in Figure S6 with statistical significance being verified. In the absence of a catalyst, the T_g increases slightly with repeated processing; with the addition of a catalyst, the T_g decreases with repeated processing where this trend magnifies with increasing catalyst concentration. We postulate that the increase in T_g without a catalyst present can be due to many factors, such as the removal of water and residual curing, which will be discussed in greater detail later. In contrast, the surprising decrease in T_g with repeated HP and in the presence of a catalyst is more complicated and is indicative of some degradation of material properties. While the same processes described for samples without a catalyst are occurring in the presence of a catalyst (i.e., water removal and residual curing), there is clearly some other dominant, competing mechanism driving a reduction of the T_g.

To test this, we performed a cycle of experiments on samples with either no catalyst or a 5 mol % catalyst concentration. The samples were cycled between temperature sweeps in DMA and either HP with applied pressure or thermal annealing (A) without applied pressure. The HP and A steps were performed at 200 °C for 1 h; DSC was done between each processing step to track changes in the T_g. As seen in Figure 3d, the T_g again increases or decreases with processing for samples without and with a catalyst, respectively, when cycled between DMA and HP.

Of greater interest, the temperature sweep results between each HP are seen for samples without (cf. Figure 3b,c) and with (cf. Figure 3e,f) a catalyst. For samples without a catalyst, the storage modulus and tan(δ) curves are almost identical regardless of processing, which agrees well with the previous literature.[2,15,17,25,27,28,31,37,38] In contrast, in the presence of a catalyst, the storage modulus decreases with processing and the tan(δ) broadens as indicated by the arrows in Figure 3. While some of the previous literature have alluded to this change,[5,29,34,39,40] it signifies an increase in the heterogeneity of the polymer network and suggests that there is some shortening of the primary chain or reduction in crosslink density. We postulate that this change is due to undesired network structure modification (e.g., an increase in free volume). The application of heat and compressive stress

https://doi.org/10.1021/acsomega.2c02677
ACS Omega 2022, 7, 29125−29134

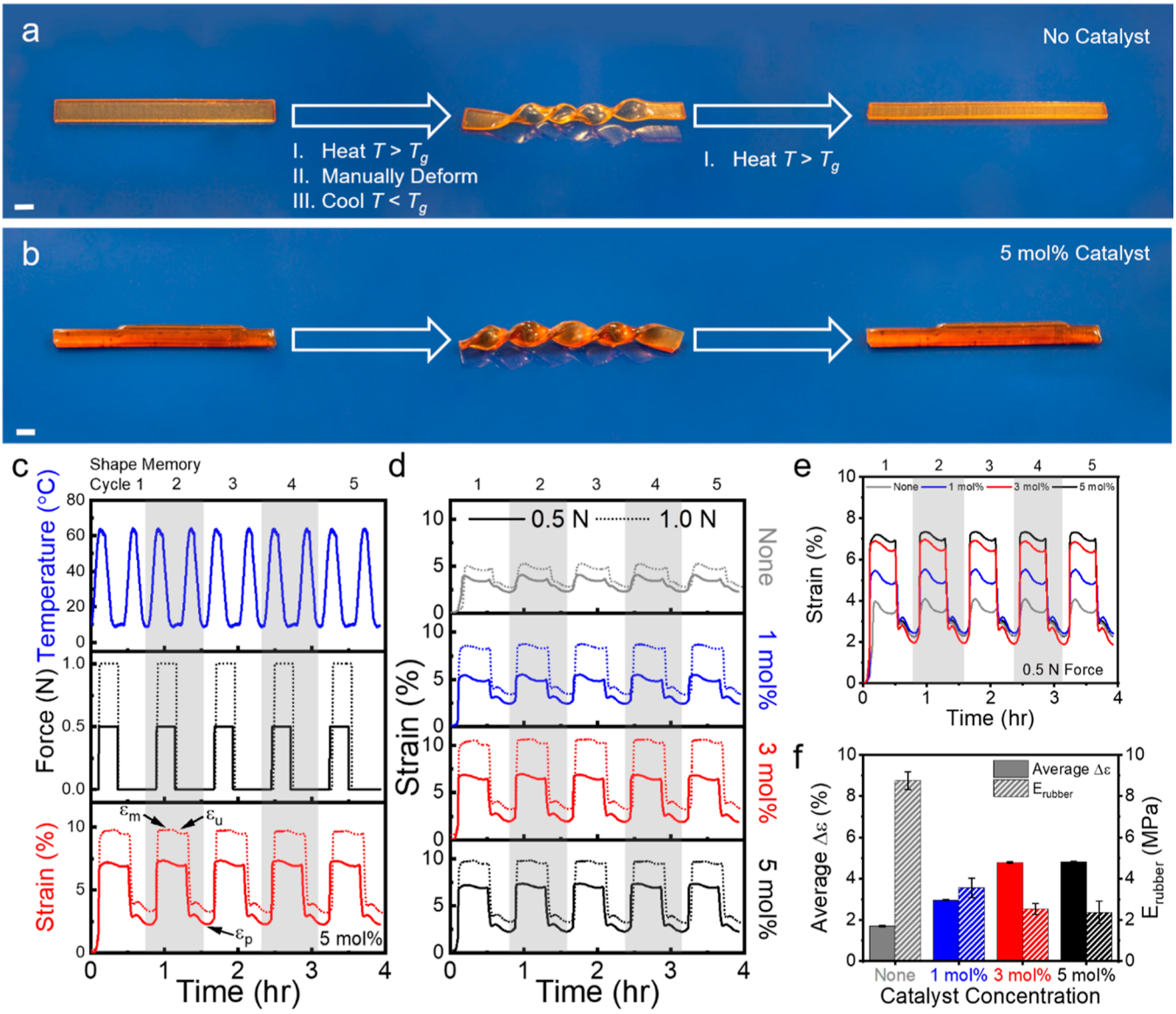

Figure 5. Shape memory demonstrations are performed for samples with either no catalyst (a) or a 5 mol % catalyst concentration (b). The scale bars are 5 mm. (c) A series of five shape memory cycles are performed where the temperature and force are controlled, and the strain is recorded; even numbered cycles are shaded gray for clarity. (d) Shape memory results are shown for a variety of catalyst concentrations with two applied forces (0.5 and 1.0 N force). In all cases, the change in strain increases with increasing force on the sample. (e) Shape memory results are compiled demonstrating that the change in strain increases with increasing catalyst concentration. (f) These results are quantified and validated by the decrease in the storage modulus of the rubbery regime with increasing catalyst concentration.

appears to enhance the interaction between the catalyst and the network, allowing for greater network rearrangement. This is further supported by previous research, which has demonstrated that the transesterification reaction is stress-favored. It should also be noted that the ΔT_g reported via DSC is mirrored in the DMA results, and these trends continue to persist with repeated numbers of cycles. To confirm that there is no significant chemical change taking place with the presence of compressive stress, we report FTIR on a pristine and processed sample, showing negligible changes (cf. Figure S7).

To confirm the importance of compressive stress, we repeated this set of experiments where the samples are cycled between temperature sweeps and annealing steps. As seen in Figure 4a, in the absence of pressure, the sample without a catalyst again exhibits a slight increase in T_g; however, this time, the sample with a 5 mol % catalyst concentration also exhibits a slight increase in T_g. We postulate that without the compressive stress on the sample, there are minimal changes in free volume and the polymer network is not significantly changed. This claim is supported by the storage modulus and tan(δ) of the annealed samples (cf. Figure 4b,c,e,f). In this case, there is some initial increase in T_g and storage modulus with one annealing step coupled with a sharpening of the tan(δ) curve; this sharpening of the tan(δ) curve points toward an increase in the homogeneity of the network structure, which we postulate is a result of water removal and some residual curing. However, any change in the material property becomes negligible with repeated cycling. Such a change in T_g has previously been reported for thermoplastics, where it was attributed to nonequilibrium voids trapped in the sample.[41] While our study clearly confirms the importance of

https://doi.org/10.1021/acsomega.2c02677
ACS Omega 2022, 7, 29125−29134

Table 1. R_r and R_f Reported for All Catalyst Concentrations as Gathered from the Set of Five Shape Memory Cycles (Columns 2−3, Figure 5e)[a]

	After Five Shape Memory Cycles		After Final Shape Reconfigurability Cycle			After Final Shape Memory Cycle	
Catalyst Concentration	R_r	R_f	R_r	R_f	$\frac{\varepsilon_{u,SR}}{\varepsilon_{u,SM}}$	R_r	R_f
none	100.5%	94.5%	97.4%	54.7%	94.1%	98.5%	88.7%
1 mol %	99.7%	93.0%	93.1%	62.9%	93.7%	98.4%	91.3%
3 mol %	99.9%	87.1%	25.2%	93.1%	164.0%	99.5%	98.2%
5 mol %	99.9%	84.3%	12.7%	97.9%	182.2%	99.7%	99.4%

[a] R_r and R_f are also reported for the final shape reconfigurability and shape memory cycle as taken from the shape reconfigurability experiments (Figure 6d)

compressive stress on changes in the network structure, additional research must be done to fully quantify its impact.

In addition to T_g, we also quantify the change in the molecular weight between crosslinks (M_c) reported with cyclic processing as calculated from the storage modulus (cf. Figure 4d).[42,43] The subsequent increase or decrease in M_c mirrors the trends found for T_g in DSC, verifying the importance of processing conditions on the network structure. When compressive stress is applied to a sample with a 5 mol % catalyst concentration, the M_c increases; while the volume variations should be small, they clearly lead to large changes in local dynamics, prompting the noticeable changes in the T_g.

To confirm that the degradation of mechanical properties and T_g is not a result of material degradation due to temperature, we performed a series of thermal degradation studies via thermogravimetric analysis (TGA), as seen in Figure S8. The material exhibits negligible degradation (<5 wt %) at temperatures $T \leq T_v$ for all catalyst concentrations up to 4 h. In addition, there is a negligible difference between nitrogen and ambient environments (cf. Figures S9 and S10); this distinction is critical as thermomechanical tests are conducted under nitrogen environments while annealing and HP are performed under atmospheric conditions. We also report the thermal degradation values for 1 h, which is the time required for a single processing step. Finally, we should note that there is an initial drop in weight retention for these TGA curves indicative of water removal, as evidenced by cyclic thermal profiles seen in Figure S11.

Shape Memory. In addition to self-healing, it is important to understand how the experimental and compositional parameters impact shape memory behavior. Qualitatively, shape memory behavior is exhibited for samples without and with a catalyst, as seen in Figure 5a,b, respectively. The shape memory behavior relies on cycling above and below the T_g; therefore, the presence of a catalyst (and the transesterification reaction) does not appear to play a role.

To quantify the shape memory capabilities, we performed a series of five shape memory cycles in DMA where the temperature and the applied force are controlled, and the resulting sample strain is monitored (cf. Figure 5c).[16,44] The temperature is cycled 25 °C above and below the T_g, and temporary strain is embedded into the material with applied forces of either 0.5 N (solid lines) or 1.0 N (dotted lines). Shape memory cycles are performed for all catalyst concentrations, as seen in Figure S12, while a single cycle is plotted in Figure S13 for clarity. Figure 5d shows that increasing the applied force on the sample increases the resulting strain per cycle, while Figure 5e shows that increasing the catalyst concentration increases the resulting strain per cycle.

These trends can be explained by the increased deformation with a higher applied load and the average storage modulus in the rubbery regime (E_{rubber} as measured via DMA), which decreases with increasing catalyst concentration (cf. Figure 5f). As previously mentioned, the crosslink density, and therefore the T_g, is indirectly related to the catalyst concentration (cf. Figure S2);[11,45−47] as the crosslink density and the E_{rubber} are directly related, we postulate that the relationship between catalyst loading and strain input during shape memory are fundamentally a result of crosslink density. To account for the noted difference in T_g with catalyst concentration, Figure S14 shows how the shape memory behavior changes as the set point maximum temperature varies above the T_g. Strain input increases slightly as the maximum temperature increases, but the catalyst concentration is the clear dominant factor determining strain input. It should also be noted that this shape memory behavior can be cycled many times; a total of 25 shape memory cycles are reported for samples without and with a catalyst as seen in Figure S15a and S15b, respectively, showing no degradation in properties.

Additionally, we quantify shape memory behavior by reporting the shape recovery (R_r) and shape fixity (R_f) ratios. R_r measures a material's ability to retain its permanent shape, while R_f measures a material's ability to temporarily fix any newly introduced mechanical deformation.[26,44,48] These values are calculated as eqs 1 and 2,

$$R_r(N) = \frac{\varepsilon_m(N) - \varepsilon_p(N)}{\varepsilon_m(N) - \varepsilon_p(N-1)} \times 100 \quad (1)$$

$$R_f(N) = \frac{\varepsilon_u(N)}{\varepsilon_m(N)} \times 100 \quad (2)$$

where N represents the cycle number, ε_m is the maximum strain at T_{max}, ε_p is the strain of the sample in the stress-free state before stress application at T_{min}, and ε_u is the strain on the sample in the stress-free state after the N^{th} programming step at T_{min}.[26,48] Note in this case that $T_{min} < T_g < T_{max}$. We demonstrate all R_r values are >99%, regardless of catalyst concentration, as seen in Table 1. Essentially, this indicates that while the amount of strain embedded is dependent upon catalyst concentration (due to the lower T_g and modulus), the ability to embed and release this strain is catalyst-independent. However, we should note that the R_f values are all >84%, with an inverse relationship between the catalyst concentration and R_f. We postulate this lower R_f value is due to some finite amount of thermal contraction coupled with issues in

https://doi.org/10.1021/acsomega.2c02677
ACS Omega 2022, 7, 29125−29134

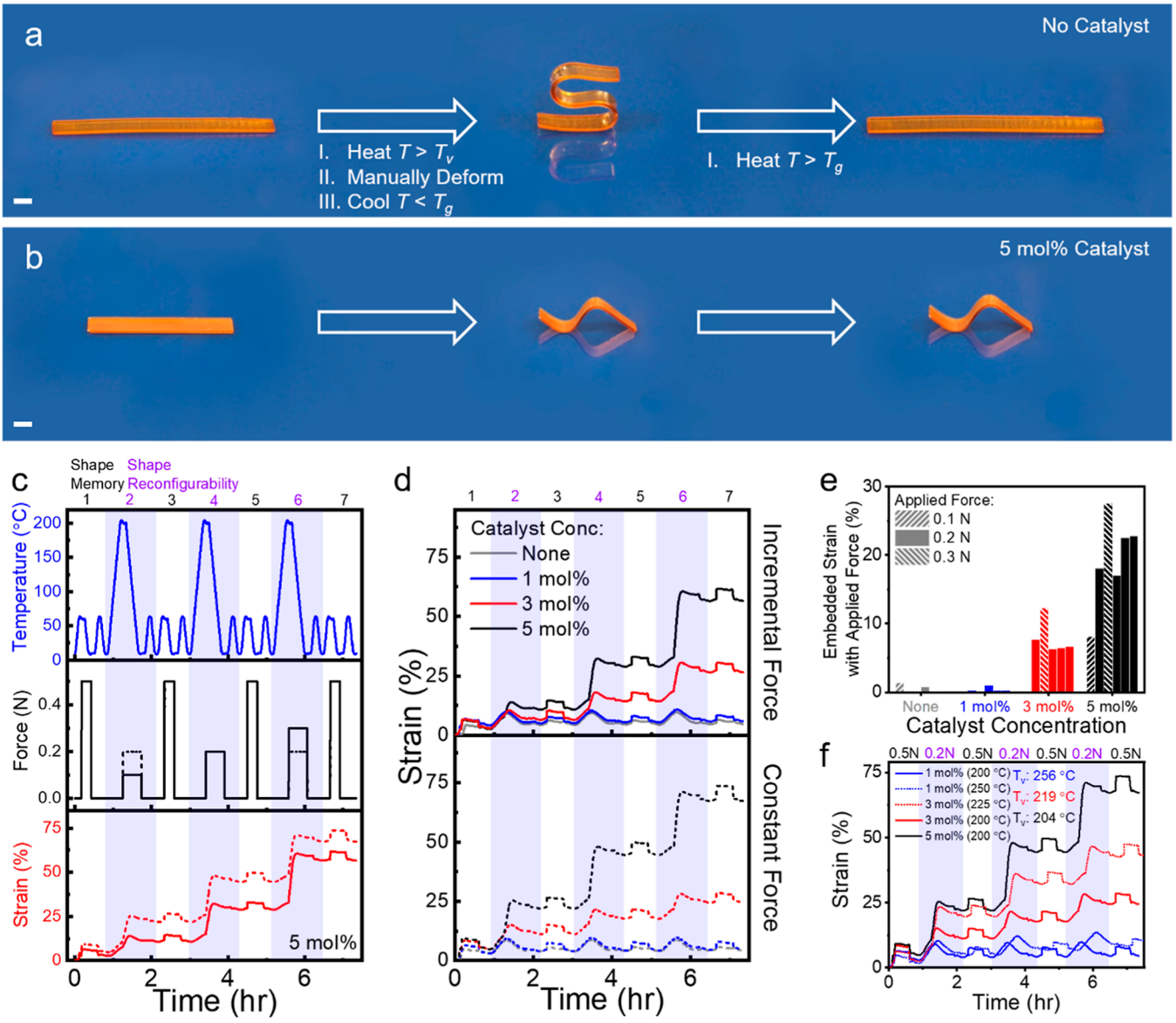

Figure 6. Shape reconfigurability demonstrations are performed for samples with either no catalyst (a) or a 5 mol % catalyst concentration (b) where the demonstrations are unsuccessful in the absence of a catalyst. The scale bars are 5 mm. (c) A series of alternating shape memory and shape reconfigurability cycles are performed where the temperature and force are controlled, and the strain is recorded; all shape memory cycles are shaded light blue for clarity. (d) Results are shown for a variety of catalyst concentrations where the applied force during shape reconfigurability cycles is either incrementally increasing or held constant. (e) In all cases, the permanently embedded strain increases with increasing force on the sample and catalyst concentration. When the force is kept constant, there is a slight increase in embedded strain. The first three bars for each sample type are recorded from the upper graph of Figure 6d, while the last three bars for each sample type are recorded from the lower graph of Figure 6d. (f) Shape reconfigurability tests are repeated where samples with either a 1 mol % or a 3 mol % catalyst concentration are heated near their T_v of 256 and 219 °C, respectively.[11]

temperature uniformity magnified by the large sample thickness.

Shape Reconfigurability. Finally, we explore the shape reconfigurability of these materials as a function of catalyst concentration and processing conditions, which, to the authors' knowledge, has not been previously reported. Reconfigurability, similarly to self-healing, is found to be catalyst-dependent as the mechanism is based on the dynamic covalent bond exchange reaction, unlike shape memory, which is a function of polymer chain rearrangement in the rubbery regime. In other words, shape memory involves cycling above and below the T_g to embed temporary strain, while shape reconfigurability involves cycling above and below the T_v to modify the permanent shape. Qualitatively, we see in Figure 6a,b that shape reconfigurability fails for samples in the absence of a catalyst, whereas it succeeds for a sample with a 5 mol % catalyst concentration, respectively. We should note that there is no true T_v for samples without a catalyst, as previously reported;[11] in this case, the T_v for samples with a 5 mol % catalyst concentration (200 °C) is utilized for all samples for demonstrative purposes.

To quantify the shape reconfigurability of these materials, we performed studies on all catalyst concentrations where we control the temperature and applied force and monitor the strain (cf. Figure 6c and S16).[16,18,25,26] A shape memory cycle (white background) is performed between each shape

https://doi.org/10.1021/acsomega.2c02677
ACS Omega 2022, 7, 29125−29134

reconfigurability cycle (light blue background) to verify that the strain embedded is indeed permanent (cf. Figure S17). The applied force during each shape reconfigurability cycle either incrementally increases by 0.1 N from 0.1 to 0.3 N with each cycle (solid lines) or it is kept constant at 0.2 N for each cycle (dashed lines), as seen in Figure 6d. The applied force for each shape memory cycle is 0.5 N. The amount of permanently embedded strain clearly increases with increasing catalyst concentration and applied force (cf. Figure 6e); when the force is kept constant for each shape reconfigurability cycle, there is a slight increase in the embedded strain due to a shrinking cross-sectional area, resulting in a slightly increasing stress on the sample.

To confirm the importance of catalyst concentration, a shape reconfigurability cycle was performed for samples with 1 mol % and 3 mol % catalyst concentrations at temperatures of 250 and 225 °C, respectively. This was done so that the experiments were performed near the T_v of each respective catalyst concentration[11] (cf. Figure S1a); regardless of this change, we see that increasing the catalyst concentration increases the amount of the final embedded strain (cf. Figure 6f) without varying the stress on the sample. Again, we postulate this is due to the fact that the number of transesterification reactions increases per unit volume and time with increasing catalyst concentration.

Quantitatively, we can calculate the R_r and R_f for the final shape reconfigurability and shape memory cycles plotted as cycles 6 and 7, respectively, in the upper portion of Figure 6d. These values, reported in Table 1, clearly show a decreasing R_r with increasing catalyst concentration for the shape reconfigurability cycles; the opposing trend is seen for R_f. These trends make perfect sense as a new, permanent shape is being fixed into the material for higher catalyst concentrations. One would expect R_r to decrease since an entirely new "permanent" shape is being programmed; contrastingly, one would expect R_f to increase as it can "fix" this new, permanent mechanical deformation.

To take this one step further, we have also calculated the ratio between ε_u as taken from subsequent shape reconfigurability and shape memory cycles. In this case, if no new shape was being fixed, one would expect this ratio to be ∼100%, which holds true for samples with low catalyst concentrations. However, as the catalyst concentration increases, this ratio increases closer to 200%, indicating that a significant amount of new strain is being permanently embedded.

Finally, we also report in Table 1 R_r and R_f values close to 100% for the final shape memory cycle. These high values indicate that the ability to undergo shape memory is not impacted by the addition of permanent strain.

CONCLUSIONS

Herein, we demonstrated the impact of compositional and environmental conditions on the reprocessability of vitrimer materials. While increasing the catalyst concentration increases the ability of vitrimer materials to undergo shape reconfigurability and self-healing, neither process is possible in the absence of a catalyst, as the transesterification reaction is the underlying mechanism. In contrast, a vitrimer's shape memory capabilities are catalyst-independent (R_r > 99%), while the amount of temporary strain embedded increases with increasing catalyst concentration (R_f decreases with increasing catalyst concentration).

However, while increasing the catalyst concentration increases the applicability of these materials, it also increases their susceptibility to processing conditions, notably compressive stress. This is evidenced by the decrease in crosslink density and T_g as a function of thermomechanical cycling for samples with a 5 mol % catalyst concentration. This degradation in properties is not seen for samples without a catalyst. In addition, we confirm that the compressive stress on the sample is responsible for this degradation by performing thermal stability studies and cycling between temperature sweeps and annealing steps. It is crucial to understand how these processing conditions impact the overall network structure and thermomechanical properties of vitrimers before their far-reaching application space can be truly explored.

MATERIALS AND METHODS

Vitrimer Synthesis. The components for our vitrimer materials were bisphenol A diglycidyl ether (DGEBA), as purchased from Sigma, along with sebacic acid (SA, 99%) and 1,5,7-triazabicyclo[4.4.0]de-5-ene (TBD), as purchased from Aldrich. All vitrimers in this study were synthesized in-house and prepared according to our previously reported methodology.[11] Silicone molds were used to generate either bars or dog bone shapes; bars were made with dimensions l × w × h: 60 mm × 6 mm × 1 mm, while dog bone shapes were made according to ASTM D638-14 (Type V). All samples were polished to remove any imperfections prior to testing.

Vitrimer Characterization. Non-isothermal creep and temperature sweep experiments were performed using a TA Instruments Discovery hybrid rheometer (DHR-III) in tension mode under a nitrogen environment. The sample gap distance was 15 mm in all cases. For non-isothermal creep experiments, the applied axial force was 0.5 N, while the sample was heated from 25 to 300 °C at a temperature ramp rate of 5 °C min^{-1}. For temperature sweep experiments, an axial strain of 0.01% was applied at a frequency of 1 Hz, while the sample was heated from 25 to 150 °C at a temperature ramp rate of 5 °C min^{-1}.

Tensile tests were performed using an MTS Insight electromechanical testing machine; all tests were performed at room temperature with a strain rate of 2 mm min^{-1}. The modulus value was recorded as the slope of the stress−strain curve over the initial 0.2% strain.

DSC was performed using a TA Instruments Discovery Series DSC 2500. All runs were performed under a nitrogen environment with temperatures cycling between 10 and 200 °C, with a temperature ramp rate of 5 °C min^{-1}. The T_g was recorded as the inflection point of the second heating curve.

Thermal stability experiments were performed using a TA Instruments TGA Q500 series under either a nitrogen or an air environment. Samples were heated at a temperature ramp rate of 10 °C min^{-1} to their respective set point temperature, where a 4 h isotherm was applied.

Shape memory and shape reconfigurability experiments were performed using a TA Instruments Discovery DMA 850 in tension mode under a nitrogen environment. The samples were cycled between 10 °C and either 60 °C or 200 °C, depending on the experiment, at a temperature ramp rate of 10 °C min^{-1}. The axial force applied on the sample varied from 0.1 to 1.0 N, with a force ramp rate of 1.0 N min^{-1}, and is specified for each test.

Fourier transform infrared spectroscopy (FTIR) was performed using a Nicolet 380 FTIR to show no significant

https://doi.org/10.1021/acsomega.2c02677
ACS Omega 2022, 7, 29125−29134

chemical change in the material with processing, regardless of catalyst concentration.

Processing Conditions. Processed samples were either hot pressed in a 30 ton Wabash hydraulic press or were annealed in a standard oven. For HP (cf. Figure S4), samples were placed back into their silicone mold (for alignment purposes) and placed between Kapton sheeting and metal plates. This entire sample was then placed between the two platens of the Wabash press, heated to 200 °C, for the specified values of time and normal pressure. For annealing, the samples were placed back into their silicone mold and simply heated in an oven at 200 °C for 1 h.

■ ASSOCIATED CONTENT

Supporting Information

The Supporting Information is available free of charge at https://pubs.acs.org/doi/10.1021/acsomega.2c02677.

Detailed description of the characterization methods used, representative non-isothermal creep results, mechanical testing results, calculated molecular weight between crosslinks, samples showing self-healing demonstrations, schematics of the apparatus used for HP damaged samples, samples showing healing process attempted with no applied pressure, representative DSC curves, *P*-values reported for the T_g values, and FTIR results (PDF)

■ AUTHOR INFORMATION

Corresponding Authors

Amber M. Hubbard − *Materials and Manufacturing Directorate and National Research Council Research Associate, Air Force Research Laboratory, Wright Patterson Air Force Base, Ohio 45433, United States*; Email: hubbard.amber.m@gmail.com

Dhriti Nepal − *Materials and Manufacturing Directorate, Air Force Research Laboratory, Wright Patterson Air Force Base, Ohio 45433, United States*; orcid.org/0000-0002-0972-9960; Email: dhriti.nepal.1@us.af.mil

Authors

Yixin Ren − *Materials and Manufacturing Directorate, Air Force Research Laboratory, Wright Patterson Air Force Base, Ohio 45433, United States; ARCTOS, Beavercreek, Ohio 45432, United States*

Alireza Sarvestani − *Department of Mechanical Engineering, Mercer University, Macon, Georgia 31207, United States*; orcid.org/0000-0001-8762-7575

Dominik Konkolewicz − *Department of Chemistry and Biochemistry, Miami University, Oxford, Ohio 45056, United States*; orcid.org/0000-0002-3828-5481

Catalin R. Picu − *Department of Mechanical, Aerospace, and Nuclear Engineering, Rensselaer Polytechnic Institute, Troy, New York 12180, United States*

Ajit K. Roy − *Materials and Manufacturing Directorate, Air Force Research Laboratory, Wright Patterson Air Force Base, Ohio 45433, United States*

Vikas Varshney − *Materials and Manufacturing Directorate, Air Force Research Laboratory, Wright Patterson Air Force Base, Ohio 45433, United States*; orcid.org/0000-0002-2613-458X

Complete contact information is available at: https://pubs.acs.org/10.1021/acsomega.2c02677

Author Contributions

A.M.H., Y.R., and D.N. were involved in project conceptualization and developing testing methodologies. A.M.H. and Y.R. were involved in the research investigation. A.M.H. wrote the initial draft of the article. All authors were involved in the review and editing process. A.S., D.K., C.P., A.R., V.V., and D.N. supervised the project.

Notes

The authors declare no competing financial interest.

■ ACKNOWLEDGMENTS

The authors thank Dr. Ming-Jen Pan and Dr. Kenneth Caster of the Air Force Office of Scientific Research (AFOSR). A. M. Hubbard would also like to thank Matthew Baczkowski for helpful discussions regarding shape memory testing procedures. In addition, this research was performed, while A. M. Hubbard held an NRC Research Associateship award at the Air Force Research Laboratory.

■ REFERENCES

(1) Wang, S.; Ma, S.; Cao, L.; Li, Q.; Ji, Q.; Huang, J.; Lu, N.; Xu, X.; Liu, Y.; Zhu, J. Conductive vitrimer nanocomposites enable advanced and recyclable thermo-sensitive materials. *J. Mater. Chem. C* **2020**, *8*, 11681−11686.

(2) Liu, Y.-Y.; Liu, G.-L.; Li, Y.-D.; Weng, Y.; Zeng, J.-B. Biobased High-Performance Epoxy Vitrimer with UV Shielding for Recyclable Carbon Fiber Reinforced Composites. *ACS Sustainable Chem. Eng.* **2021**, *9*, 4638−4647.

(3) Samanta, S.; Kim, S.; Saito, T.; Sokolov, A. P. Polymers with Dynamic Bonds: Adaptive Functional Materials for a Sustainable Future. *J. Phys. Chem. B* **2021**, *125*, 9389−9401.

(4) Liu, T.; Zhao, B.; Zhang, J. Recent development of repairable, malleable and recyclable thermosetting polymers through dynamic transesterification. *Polymer* **2020**, *194*, 122392.

(5) Li, L.; Chen, X.; Jin, K.; Torkelson, J. M. Vitrimers Designed Both To Strongly Suppress Creep and To Recover Original Cross-Link Density after Reprocessing: Quantitative Theory and Experiments. *Macromolecules* **2018**, *51*, 5537−5546.

(6) Fortman, D. J.; Brutman, J. P.; De Hoe, G. X.; Snyder, R. L.; Dichtel, W. R.; Hillmyer, M. A. Approaches to Sustainable and Continually Recyclable Cross-Linked Polymers. *ACS Sustainable Chem. Eng.* **2018**, *6*, 11145−11159.

(7) Qiu, J.; Ma, S.; Wang, S.; Tang, Z.; Li, Q.; Tian, A.; Xu, X.; Wang, B.; Lu, N.; Zhu, J. Upcycling of Polyethylene Terephthalate to Continuously Reprocessable Vitrimers through Reactive Extrusion. *Macromolecules* **2021**, *54*, 703−712.

(8) Krishnakumar, B.; Sanka, R. V. S. P.; Binder, W. H.; Parthasarthy, V.; Rana, S.; Karak, N. Vitrimers: Associative dynamic covalent adaptive networks in thermoset polymers. *Chem. Eng. J.* **2020**, *385*, 123820−123833.

(9) Denissen, W.; Winne, J. M.; Du Prez, F. E. Vitrimers: permanent organic networks with glass-like fluidity. *Chem. Sci.* **2016**, *7*, 30−38.

(10) Kaiser, S.; Novak, P.; Giebler, M.; Gschwandl, M.; Novak, P.; Pilz, G.; Morak, M.; Schlögl, S. The crucial role of external force in the estimation of the topology freezing transition temperature of vitrimers by elongational creep measurements. *Polymer* **2020**, *204*, 122804−122813.

(11) Hubbard, A. M.; Ren, Y.; Konkolewicz, D.; Sarvestani, A.; Picu, C. R.; Kedziora, G. S.; Roy, A.; Varshney, V.; Nepal, D. Vitrimer Transition Temperature Identification: Coupling Various Thermomechanical Methodologies. *ACS Appl. Polym. Mater.* **2021**, *3*, 1756−1766.

(12) De Alwis Watuthanthrige, N.; Ahammed, B.; Dolan, M. T.; Fang, Q.; Wu, J.; Sparks, J. L.; Zanjani, M. B.; Konkolewicz, D.; Ye, Z. Accelerating dynamic exchange and self-healing using mechanical forces in crosslinked polymers. *Mater. Horiz.* **2020**, *7*, 1581−1587.

(13) Liu, W.; Schmidt, D. F.; Reynaud, E. Catalyst Selection, Creep, and Stress Relaxation in High-Performance Epoxy Vitrimers. *Ind. Eng. Chem. Res.* **2017**, *56*, 2667−2672.
(14) Capelot, M.; Unterlass, M. M.; Tournilhac, F.; Leibler, L. Catalytic Control of the Vitrimer Glass Transition. *ACS Macro Lett.* **2012**, *1*, 789−792.
(15) Lossada, F.; Zhu, B.; Walther, A. Dry Processing and Recycling of Thick Nacre−Mimetic Nanocomposites. *Adv. Funct. Mater.* **2021**, *31*, 2102677.
(16) Yang, Z.; Wang, Q.; Wang, T. Dual-Triggered and Thermally Reconfigurable Shape Memory Graphene-Vitrimer Composites. *ACS Appl. Mater. Interfaces* **2016**, *8*, 21691−21699.
(17) Si, H.; Zhou, L.; Wu, Y.; Song, L.; Kang, M.; Zhao, X.; Chen, M. Rapidly reprocessable, degradable epoxy vitrimer and recyclable carbon fiber reinforced thermoset composites relied on high contents of exchangeable aromatic disulfide crosslinks. *Composites, Part B* **2020**, *199*, 108278.
(18) Montarnal, D.; Capelot, M.; Tournilhac, F.; Leibler, L. Silica-Like Malleable Materials from Permanent Organic Networks. *Science* **2011**, *334*, 965−968.
(19) Yang, Y.; Zhang, S.; Zhang, X.; Gao, L.; Wei, Y.; Ji, Y. Detecting topology freezing transition temperature of vitrimers by AIE luminogens. *Nat. Commun.* **2019**, *10*, 3165−3172.
(20) Fang, H.; Ye, W.; Ding, Y.; Winter, H. H. Rheology of the Critical Transition State of an Epoxy Vitrimer. *Macromolecules* **2020**, *53*, 4855−4862.
(21) Guerre, M.; Taplan, C.; Winne, J. M.; Du Prez, F. E. Vitrimers: directing chemical reactivity to control material properties. *Chem. Sci.* **2020**, *11*, 4855−4870.
(22) Zhang, B.; Digby, Z. A.; Flum, J. A.; Chakma, P.; Saul, J. M.; Sparks, J. L.; Konkolewicz, D. Dynamic Thiol−Michael Chemistry for Thermoresponsive Rehealable and Malleable Networks. *Macromolecules* **2016**, *49*, 6871−6878.
(23) Li, G.; Zhang, P.; Huo, S.; Fu, Y.; Chen, L.; Wu, Y.; Zhang, Y.; Chen, M.; Zhao, X.; Song, P. Mechanically Strong, Thermally Healable, and Recyclable Epoxy Vitrimers Enabled by ZnAl-Layer Double Hydroxides. *ACS Sustainable Chem. Eng.* **2021**, *9*, 2580−2590.
(24) Niu, W.; Cao, X.; Wang, Y.; Yao, B.; Zhao, Y.; Cheng, J.; Wu, S.; Zhang, S.; He, X. Photonic Vitrimer Elastomer with Self-Healing, High Toughness, Mechanochromism, and Excellent Durability based on Dynamic Covalent Bond. *Adv. Funct. Mater.* **2021**, *31*, 2009017.
(25) Trejo-Machin, A.; Puchot, L.; Verge, P. A cardanol-based polybenzoxazine vitrimer: recycling, reshaping and reversible adhesion. *Polym. Chem.* **2020**, *11*, 7026−7034.
(26) Wang, D. H.; Tan, L.-S. Origami-Inspired Fabrication: Self-Folding or Self-Unfolding of Cross-Linked-Polyimide Objects in Extremely Hot Ambience. *ACS Macro Lett.* **2019**, *8*, 546−552.
(27) Li, L.; Chen, X.; Jin, K.; Rusayyis, M. B.; Torkelson, J. M. Arresting Elevated-Temperature Creep and Achieving Full Cross-Link Density Recovery in Reprocessable Polymer Networks and Network Composites via Nitroxide-Mediated Dynamic Chemistry. *Macromolecules* **2021**, *54*, 1452−1464.
(28) Wang, S.; Ma, S.; Li, Q.; Xu, X.; Wang, B.; Huang, K.; liu, Y.; Zhu, J. Facile Preparation of Polyimine Vitrimers with Enhanced Creep Resistance and Thermal and Mechanical Properties via Metal Coordination. *Macromolecules* **2020**, *53*, 2919−2931.
(29) Li, H.; Zhang, B.; Yu, K.; Yuan, C.; Zhou, C.; Dunn, M. L.; Qi, H. J.; Shi, Q.; Wei, Q. H.; Liu, J.; Ge, Q. Influence of treating parameters on thermomechanical properties of recycled epoxy-acid vitrimers. *Soft Matter* **2020**, *16*, 1668−1677.
(30) Zhang, B.; Li, H.; Yuan, C.; Dunn, M. L.; Qi, H. J.; Yu, K.; Shi, Q.; Ge, Q. Influences of processing conditions on mechanical properties of recycled epoxy-anhydride vitrimers. *J. Appl. Polym. Sci.* **2020**, *137*, 49246.
(31) Chen, M.; Zhou, L.; Wu, Y.; Zhao, X.; Zhang, Y. Rapid Stress Relaxation and Moderate Temperature of Malleability Enabled by the Synergy of Disulfide Metathesis and Carboxylate Transesterification in Epoxy Vitrimers. *ACS Macro Lett.* **2019**, *8*, 255−260.
(32) Hubbard, A. M.; Ren, Y.; Picu, C. R.; Sarvestani, A.; Konkolewicz, D.; Roy, A. K.; Varshney, V.; Nepal, D. Creep Mechanics of Epoxy Vitrimer Materials. *ACS Appl. Polym. Mater.* **2022**, *4*, 4254−4263.
(33) Farge, L.; Hoppe, S.; Daujat, V.; Tournilhac, F.; André, S. Solid Rheological Properties of PBT-Based Vitrimers. *Macromolecules* **2021**, *54*, 1838−1849.
(34) Zhang, B.; Yuan, C.; Zhang, W.; Dunn, M. L.; Qi, H. J.; Liu, Z.; Yu, K.; Ge, Q. Recycling of vitrimer blends with tunable thermomechanical properties. *RSC Adv.* **2019**, *9*, 5431−5437.
(35) Zhang, L.; Liu, Z.; Wu, X.; Guan, Q.; Chen, S.; Sun, L.; Guo, Y.; Wang, S.; Song, J.; Jeffries, E. M.; He, C.; Qing, F. L.; Bao, X.; You, Z. A Highly Efficient Self-Healing Elastomer with Unprecedented Mechanical Properties. *Adv. Mater.* **2019**, *31*, 1901402.
(36) Elling, B. R.; Dichtel, W. R. Reprocessable Cross-Linked Polymer Networks: Are Associative Exchange Mechanisms Desirable? *ACS Cent. Sci.* **2020**, *6*, 1488−1496.
(37) Feng, Z.; Yu, B.; Hu, J.; Zuo, H.; Li, J.; Sun, H.; Ning, N.; Tian, M.; Zhang, L. Multifunctional Vitrimer-Like Polydimethylsiloxane (PDMS): Recyclable, Self-Healable, and Water-Driven Malleable Covalent Networks Based on Dynamic Imine Bond. *Ind. Eng. Chem. Res.* **2019**, *58*, 1212−1221.
(38) Zhou, Y.; Goossens, J. G. P.; Sijbesma, R. P.; Heuts, J. P. A. Poly(butylene terephthalate)/Glycerol-based Vitrimers via Solid-State Polymerization. *Macromolecules* **2017**, *50*, 6742−6751.
(39) Condo, P. D.; Sanchez, I. C.; Panayiotou, C. G.; Johnston, K. P. Glass Transition Behavior Including Retrograde Vitrification of Polymers with Compressed Fluid Diluents. *Macromolecules* **1992**, *25*, 6119−6127.
(40) Lessard, J. J.; Scheutz, G. M.; Hughes, R. W.; Sumerlin, B. S. Polystyrene-Based Vitrimers: Inexpensive and Recyclable Thermosets. *ACS Appl. Polym. Mater.* **2020**, *2*, 3044−3048.
(41) Hub, C.; Harton, S. E.; Hunt, M. A.; Fink, R.; Ade, H. Influence of sample preparation and processing on observed glass transition temperatures of polymer nanocomposites. *J. Polym. Sci., Part B: Polym. Phys.* **2007**, *45*, 2270−2276.
(42) Kuang, X.; Liu, G.; Dong, X.; Wang, D. Correlation between stress relaxation dynamics and thermochemistry for covalent adaptive networks polymers. *Mater. Chem. Front.* **2017**, *1*, 111−118.
(43) Treloar, L. R. G. The elasticity and related properties of rubbers. *Rep. Prog. Phys.* **1973**, *36*, 755−826.
(44) Altuna, F. I.; Hoppe, C. E.; Williams, R. J. J. Shape memory epoxy vitrimers based on DGEBA crosslinked with dicarboxylic acids and their blends with citric acid. *RSC Adv.* **2016**, *6*, 88647−88655.
(45) Niu, X.; Wang, F.; Li, X.; Zhang, R.; Wu, Q.; Sun, P. Using Zn2+ Ionomer To Catalyze Transesterification Reaction in Epoxy Vitrimer. *Ind. Eng. Chem. Res.* **2019**, *58*, 5698−5706.
(46) Tangthana-umrung, K.; Poutrel, Q. A.; Gresil, M. Epoxy Homopolymerization as a Tool to Tune the Thermo-Mechanical Properties and Fracture Toughness of Vitrimers. *Macromolecules* **2021**, *54*, 8393−8406.
(47) Poutrel, Q.-A.; Blaker, J. J.; Soutis, C.; Tournilhac, F.; Gresil, M. Dicarboxylic acid-epoxy vitrimers: influence of the off-stoichiometric acid content on cure reactions and thermo-mechanical properties. *Polym. Chem.* **2020**, *11*, 5327−5338.
(48) Abdullah, S. A.; Jumahat, A.; Abdullah, N. R.; Frormann, L. Determination of Shape Fixity and Shape Recovery Rate of Carbon Nanotube-filled Shape Memory Polymer Nanocomposites. *Procedia Eng.* **2012**, *41*, 1641−1646.

https://doi.org/10.1021/acsomega.2c02677
ACS Omega 2022, 7, 29125−29134